2D Solitons in $\mathcal{PT}$-Symmetric Photonic Lattices

Andre L. M. Muniz, Martin Wimmer, Arstan Bisianov, and Ulf Peschel*
Abbe Center of Photonics, Friedrich Schiller University Jena, Max-Wien-Platz 1, 07743 Jena, Germany

Roberto Morandotti†
INRS-EMT, 1650 Blvd Lionel Boulet, Varennes PQ J3X 1S2, Canada

Pawel S. Jung‡ and Demetrios N. Christodoulides
CREOL, University of Central Florida, Orlando, Florida 32816-2700, USA

(Received 12 August 2019; published 18 December 2019)

Over the last few years, parity-time ($\mathcal{PT}$) symmetry has been the focus of considerable attention. Ever since, pseudo-Hermitian notions have permeated a number of fields ranging from optics to atomic and topological physics, as well as optomechanics, to mention a few. Unlike their Hermitian counterparts, nonconservative systems do not exhibit *a priori* real eigenvalues and hence unitary evolution. However, once $\mathcal{PT}$ symmetry is introduced, such dissipative systems can surprisingly display a real eigenspectrum, thus ensuring energy conservation during evolution. In optics, $\mathcal{PT}$ symmetry can be readily established by incorporating, in a balanced way, regions having an equal amount of optical gain and loss. However, thus far, all optical realizations of such $\mathcal{PT}$ symmetry have been restricted to a single transverse dimension (1D), such as arrays of optical waveguides or active coupled cavity arrangements. In most cases, only the loss function was modulated—a restrictive aspect that is only appropriate for linear systems. Here, we present an experimental platform for investigating the interplay between $\mathcal{PT}$ symmetry and nonlinearity in two-dimensional (2D) environments, where nonlinear localization and soliton formation can be observed. In contrast to typical dissipative solitons, we demonstrate a one-parameter family of soliton solutions that are capable of displaying attributes similar to those encountered in nonlinear conservative arrangements. For high optical powers, this new family of $\mathcal{PT}$ solitons tends to collapse on a discrete network—thus giving rise to an amplified, self-accelerating structure.

DOI: 10.1103/PhysRevLett.123.253903

Absorption and diffraction have always been limiting factors in fully exploiting the potential of light in both science and technology. In addressing these two fundamental problems, two main avenues have been pursued: (i) optical amplification in order to overcome losses and (ii) usage of optical solitons to compensate for dispersive forces via optical nonlinearities [1]. While each of these components alone has been successful in dealing with these issues, the combined use of these two approaches has been thus far quite challenging. This is due to the fact that any restoration of conservative features requires a delicate adjustment of the spectrum. In case this condition is not met, this leads to a decay or an explosive amplification, which is eventually limited by gain saturation [2]. In the latter scenario, dissipative solitons can appear in the system—occasionally resting on a constant background because of stability requirements. In contrast, in parity-time ($\mathcal{PT}$)-symmetric systems [3,4], it is possible to restore a quasiconservative setting that is free of such constraints. In recent years, several studies have shown that optical systems endowed with $\mathcal{PT}$ symmetry can enable unusual and previously unattainable light propagation features [5–23]. These include, among others, double refraction and band merging [6,13], unidirectional invisibility [11,23], abrupt phase transitions and power oscillations [5,24], as well as unidirectional propagation [5,10,11], to mention a few. Naturally, by introducing nonlinearity, one could expect an even richer ground for new and unexpected phenomena. In this respect, it has been suggested, in a number of works, that entire soliton families do exist in one- and two-dimensional $\mathcal{PT}$-symmetric arrangements with Kerr nonlinearities [13,18,25]. However, an experimental observation of such effects is still lacking—especially in 2D periodic configurations where soliton behavior depends critically on the lattice dimensionality [26,27]. To some extent, one can appreciate this emerging complexity by considering the properties of the conservative nonlinear Schröedinger equation with a focusing Kerr nonlinearity [25,27]. While the soliton energy in 1D systems is inversely proportional to their width, in 2D this quantity remains constant [1,27]. Even more importantly, in the latter case, the field distribution can undergo a catastrophic collapse, as the contraction does not require additional power.

In this Letter, these intriguing properties are observed in a $\mathcal{PT}$-symmetric system, except this time the collapse is

arrested by the inherent discreteness of the lattice [28], built through an internal gain, loss and index modulation. In order to realize two-dimensional $\mathcal{PT}$-symmetric solitons, we make use of the newly developed concept of synthetic dimensions [28,29]. By combining short- and long-range interactions [30], we experimentally implement a discrete two-dimensional lattice, which features a unique class of solitonic solutions. In these lattices, we demonstrate linear and nonlinear beam evolution as well as nonlinear localization. In addition to immobile solitons, in 2D we observe self-accelerating nonlinear wave packets—an effect never reported before.

Our experimental platform [see Fig. 1(a)] is based on four slightly dissimilar paths having a fiber length of approximately 30 km. They are grouped in two pairs, each standing for one synthetic transverse dimension (see the Supplemental Material [31], Notes 1, 2), as demonstrated for 1D [16,32–35] and 2D [28,30] lattices. The two inner paths A and B differ by $\Delta L_{\text{inner}} = L_A - L_B \approx 600$ m ($\Delta T_{\text{inner}} = 3$ μs), while the two outer paths C and D differ by $\Delta L_{\text{outer}} = L_C - L_D \approx 6$ m ($\Delta T_{\text{outer}} = 30$ ns). As shown in Fig. 1(a), an initial seed pulse is injected via a fiber optical coupler into the outer left path C and splits into two pulses (step Ia and Ib) at the first 50/50 coupler at the entrance of the two inner paths A and B. After passing through the second 50/50 coupler, the pulses split again (step IIa and IIb) and propagate as pairs through the outer paths C and D. They return with varying delay at the first 50/50 coupler after a mean round trip time $T \approx 300$ μs and this process starts again. After passing path A (B), x increases (decreases) by one, which is equivalent to a step to the right (left) on the 2D synthetic lattice. Moreover, after propagating through the outer path C (D), y increases (decreases) by one, corresponding to a step up (down) on the lattice. In this way, any direction through the 2D lattice is equivalent to a combination of round-trips through the four different paths [see pathways in Fig. 1(b)] and vice versa. The pulse sequence evolving in the system is then measured by photo detectors [blue curves in Fig. 1(c)], sampled electronically [black dashed curves in the insets of Fig. 1(c)], and mapped onto a 2D discrete lattice in x and y coordinates [30] [see inset in Fig. 1(c) for time steps $m = 3$ corresponding to the section of the total time trace marked by red dashed lines].

Given that we use 22 ns long pulses, pulse dispersion is negligible [36] and the dynamics in this system are well described by the complex amplitudes $a^m_{x,y}/b^m_{x,y}$ and $c^m_{x,y}/d^m_{x,y}$ of the pulses traveling through path A and B (short or long inner paths) and path C and D (short or long outer paths), respectively. By interpreting the number of roundtrips m as a discretized time variable and the subscripts (x, y) as the Cartesian position on the synthetic lattice displayed in Fig. 1(b), the pulse evolution in the inner loop can then be described by the following equations

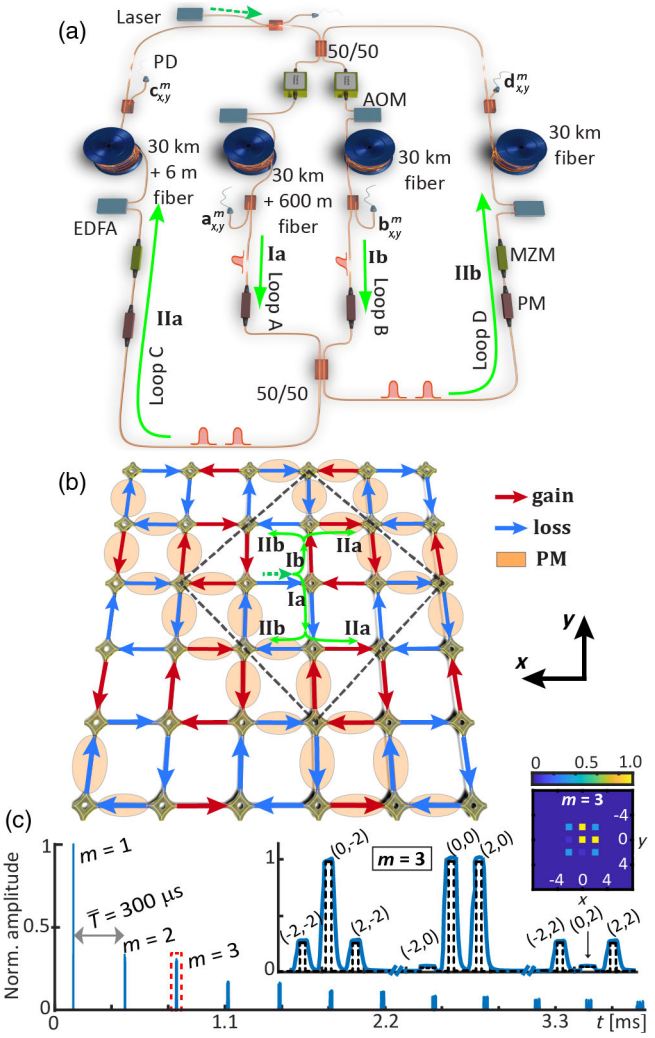

FIG. 1. Light propagation in a 2D mesh lattice. (a) The inner ($a^m_{x,y}$ and $b^m_{x,y}$) and outer ($c^m_{x,y}$ and $d^m_{x,y}$) pair of fibers are connected via 50/50 couplers. (b) The $\mathcal{PT}$-symmetric 2D synthetic lattice is virtually mapped accordingly to the arrival time of the pulses in each path (PM: phase modulation). (c) The pulse amplitudes are photodetected (blue line), sampled electronically (black dashed line), and mapped onto a 2D spatially x-y representation.

$$a^m_{x,y} = \sqrt{\frac{G'}{2}}(c^{m-1}_{x+1,y} + id^{m-1}_{x+1,y})\exp(i\varphi_a + i\chi P), \quad (1)$$

$$b^m_{x,y} = \sqrt{\frac{1}{2G'}}(d^{m-1}_{x-1,y} + ic^{m-1}_{x-1,y})\exp(i\varphi_b + i\chi P), \quad (2)$$

while in the outer loop by

$$c^m_{x,y} = \sqrt{\frac{G'}{2}}(a^m_{x,y+1} + ib^m_{x,y+1})\exp(i\varphi_c + i\chi P), \quad (3)$$

$$d^m_{x,y} = \sqrt{\frac{1}{2G'}}(b^m_{x,y-1} + ia^m_{x,y-1})\exp(i\varphi_d + i\chi P). \quad (4)$$

New pulses are formed by interference inside the 50/50 coupler as reflected by the second term of Eqs. (1)–(4). The third term represents position and round trip dependent phases φ_a, φ_b, φ_c, and φ_d imprinted by phase modulators (PM) in order to ensure 2D $\mathcal{PT}$ symmetry [26] [see Fig. 1(b) and the Supplemental Material [31], Note 9). Nonlinear phase modulation is induced by the action of the Kerr nonlinearity in the optical fiber [1], which is represented by an effective factor χ and proportional to the pulse power (P) (see the Supplemental Material [31], Note 7). G' stands for the adjustable net gain or loss [$G' = G^{(-1)^m}$] introduced by the joint action of acousto-optic (AOM) and Mach-Zehnder modulators (MZM) and erbium-doped fiber amplifiers (EDFA). For an idle transmission ratio of AOMs and MZMs of 80%, all losses of the system are compensated by EDFA, thus restoring energy conservation ($G = 1$) and enabling a considerable increase in propagation steps. Still pulses can easily be amplified [6] up to a value of $G_{\mathrm{MAX}} = 1.25$ per round trip.

In order to introduce 2D $\mathcal{PT}$ symmetry, an antisymmetric gain modulation must be imposed [26], which is here implemented by amplifying and attenuating the shorter (longer) inner and outer loops in a balanced way. Similarly, the simplest phase modulation that satisfies the 2D $\mathcal{PT}$-symmetry condition was applied, following the pattern displayed in Fig. 1(b) (see the orange marks) with a constant phase shift φ_0 (see the Supplemental Material [31], Note 6 and [37]). Interestingly, this $\mathcal{PT}$-symmetric phase modulation as depicted in Fig. 1(b) creates zigzag-shaped potential barriers along the lattice, akin to those expected from Peierls-Nabarro (PN) effects [38]. As a result of this phase and gain-loss pattern, the unit cell of the lattice is doubled [see dashed square in Fig. 1(b)] and thus the two original bands [28] of the linear spectrum split into four in total. Under linear conditions ($\chi = 0$), the band structure of our system is given by the following dispersion relation

$$\begin{aligned}\cos\theta = \pm\frac{1}{8}\Bigg(&-2\cos(g)+\cos(k^-)-4\cos(\varphi_0)\\&\times\sin^2\left(\frac{k^+}{2}\right)\pm\sqrt{2}\cos\left(\frac{k^+}{2}\right)\times[14-6\cos(2\varphi_0)\\&+4\cos(\varphi_0-g)+4\cos(\varphi_0+g)+\cos(2\varphi_0-k^-)\\&+4\cos(\varphi_0+k^-)+4\cos(\varphi_0-k^+)+4\cos(g-k^+)\\&+4\cos(g+k^-)-2\cos(k^+)+\cos(\varphi_0+k^+)]^{1/2}\Bigg),\end{aligned}\tag{5}$$

which was obtained by inserting the evolution Eqs. (1)–(4) into a Floquet-Bloch ansatz of the form $e^{-i\theta}e^{i(xk_x+yk_y)}$ [39]. Here, the phase and amplitude modulation intensities are denoted by φ_0 and $g = -2i\ln(G)$, respectively. θ stands for the propagation constant, k^+ and k^- represent, respectively, $k_x + k_y$ and $k_x - k_y$, where k_x and k_y are the Bloch quasi momenta (see the Supplemental Material [31], Notes 6, 8). In the passive (conservative) case ($G = 1.0, \varphi_a = \varphi_b = \varphi_c = \varphi_d = 0$), the systems eigenvalues are real [see Fig. 2(a)] and hence light transport performs a 2D ballistic walk [28]. However, for $G > 1.0$ and without any phase modulation, the band structure becomes complex [$\mathrm{Im}(\theta) > 0$)] and hence $\mathcal{PT}$-symmetry is broken [see Figs. 2(b) and 2(c)]—causing the power to grow exponentially during propagation, as shown in Fig. 2(e) for $\varphi_0 = 0$ and 0.3π. In order to restore pseudo-Hermiticity, the symmetric phase potential must be strong enough, so that $\mathcal{PT}$ symmetry is recovered and the average energy is conserved during propagation, which is consistent with a real-valued band structure [see Figs. 2(d) and 2(e) for $\varphi_0 = 0.6\pi$].

In the range of values where $\mathcal{PT}$ symmetry is restored, e.g., $G = 1.1$ and $\varphi_0 = 0.6\pi$, where the band structure is real [$\mathrm{Im}(\theta) = 0$] and exhibits a gap, its upper dispersion branch is similar to that associated with waves propagating in a bulk material since it has a constant positive curvature over a wide range of Bloch momenta. Importantly, a specific narrow region in the Brillouin zone can be excited using a wave packet that is relatively broad in real space. In this configuration, an excitation promoting a selective population within the central point Γ ($k_x = k_y = 0$) of the upper band is carried out by launching a train of rectangular pulses comprising of a Gaussian envelope $G_w(x, y) = A_w \exp[-(x^2 + y^2)/w^2]$ along the synthetic x and y axis [see Fig. 3(a)]; for more details concerning initial conditions, see the Supplemental Material [31], Note 10).

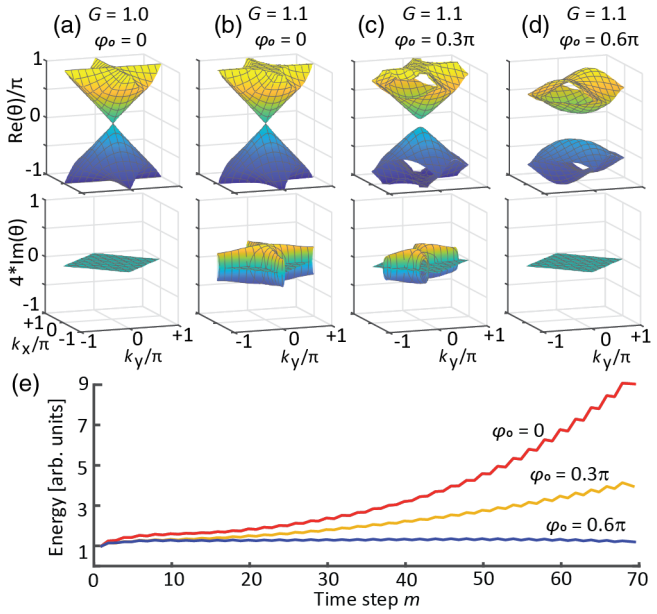

FIG. 2. Band structure of a 2D $\mathcal{PT}$-symmetric mesh lattice and its respective quasiconservative regions. (a) Passive band structure ($G = 1.0$; $\varphi_0 = 0$). (b)–(d) Band structure in the presence of gain or loss of $G = 1.1$ and phase potential φ_0 of (b) 0, (c) 0.3π, (d) 0.6π. (e) Experimental observation of the energy evolving as a function of round trips m.

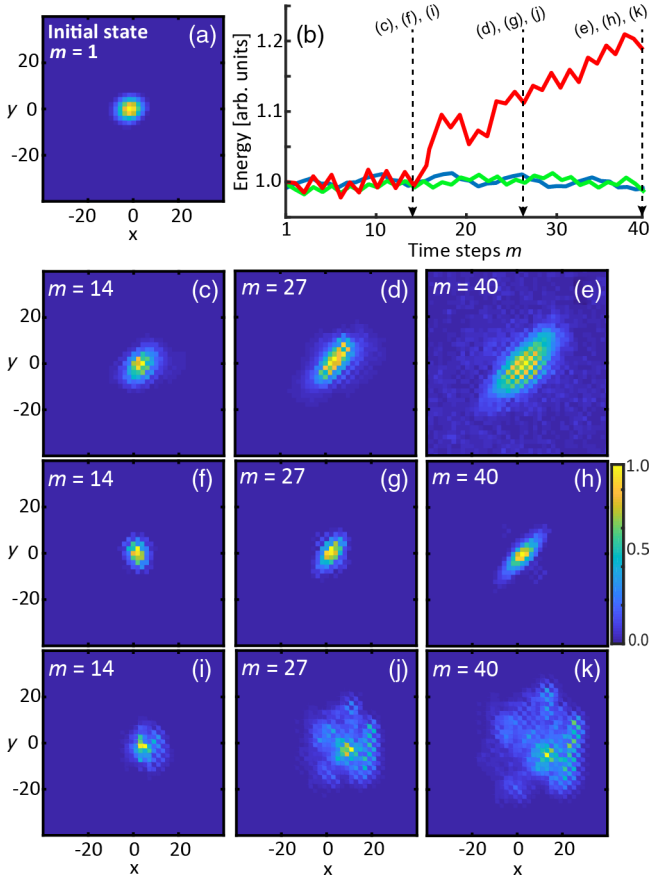

FIG. 3. Evolution of a broad excitation in the presence of $\mathcal{PT}$-symmetric potentials ($G = 1.1$, $\varphi_0 = 0.6\pi$). (a) 2D image of the initial Gaussian distribution at the input. (b) Experimental investigation of the energy evolution as a function of time steps m for 0.208 (blue), 1.1 (green), 4.15 mW (red) input power. (c)–(k) 2D image, displayed with normalized scaled colors, of the wave packets after 14 (c), (f), (i), 27 (d), (g), (j), and 40 (e), (h), (k) time steps m for different input powers (0.208,1.1 and 4.15 mW).

In this case, a variable amplitude (A_w) is used while the width (w) is fixed in such a way so as the $1/e$ drop in intensity occurs after six sites.

At an input power of approximately 0.208 mW, the field distribution experiences linear diffraction and spreads diagonally in the x-y plane in this synthetic lattice [see Figs. 3(c)–3(e)] due to the orientation of the phase potential lines [Fig. 1(b)]. By gradually increasing the input power to 1.1 mW, 2D $\mathcal{PT}$ solitons start to appear [see Figs. 3(f)–3(h)]. Numerical simulations show that in this regime, the soliton lifetime strongly depends on the soliton total energy $E_T = \sum_{x,y=0}^{N} |a_{x,y}|^2 + |b_{x,y}|^2$ and the respective gain factor. As in the case of 1D $\mathcal{PT}$ mesh lattices [13,25,26], these solitons also belong to a one-parameter family. In this respect, the 2D $\mathcal{PT}$ system studied here behaves similarly to that of its Hermitian counterpart and therefore allows the solitons to adapt their amplitudes to their widths.

Similar to Townes-like solitons in conservative 2D nonlinear Schröedinger systems [27,40], the 2D $\mathcal{PT}$-solitonic waves are intrinsically unstable. Figure 4(a) displays the dependence of the soliton propagation constant (eigenvalue θ) as a function of the total energy (E) for both a conservative ($G = 1.0$) and a non-Hermitian [3,4] lattice ($1.01 \leq G \leq 1.76$). Note that the intensity profile of low energy soliton solutions reflects the asymmetry of the lattice showing two nonequivalent diagonal directions [compare Figs. 3(e) and 3(h)]. In contrast, high energy solutions appear more symmetric in shape when their width almost approaches one elementary $\mathcal{PT}$ unit cell [see Fig. 3(h)], thus corresponding to a highly localized soliton trapped between two zigzag-shaped phase potential barriers (acting as a Peierls-Nabarro barrier [38,41]). Similarly, Fig. 4(b) depicts the eigenvalue-soliton width curve, where the field distribution along the diagonal $x = y$ was fitted with a Gaussian function. Interestingly, the conservative soliton line (dotted black line) determines the threshold of the propagation constant beyond which nonconservative nonlinear localized stationary solutions (i.e., $G > 1.0$) cannot exist. As the gain factor increases, the corresponding propagation constant curves for $\mathcal{PT}$ solitons proportionally decrease and their widths rapidly become narrower.

Also, nonconservative soliton eigenvalues present an initial total energy E_T threshold that makes them highly unstable and which immediately blows up, releasing a large amount of energy due to their higher dissipative flux of energy for bigger gain factors [see Fig. 4(c)]. Similarly, soliton maximum lifetime is quantified by the propagation time step m, at which the amplitude profile deviation $\sum_{x,y=0}^{N}(|a_{x,y}^{m+2} - e^{i\theta}a_{x,y}^{m}|^2 + |b_{x,y}^{m+2} - e^{i\theta}b_{x,y}^{m}|^2)$ between two subsequent time steps m and $m+2$ (after one modulation period) exceeds 1% of the total energy E_T

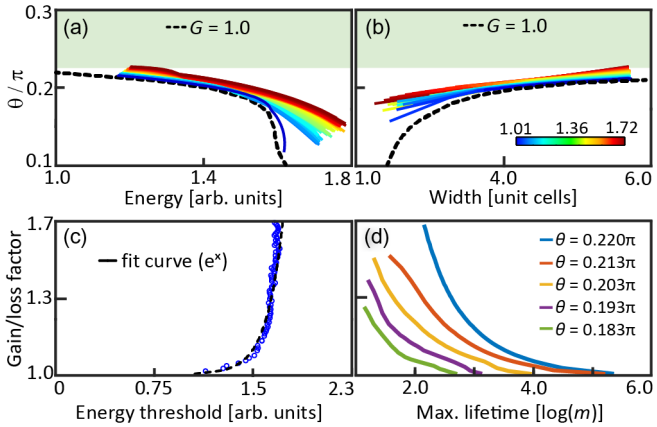

FIG. 4. Soliton simulation in conservative ($G = 1.0$) and $\mathcal{PT}$-symmetric systems ($\varphi_0 = 0.6\pi$). (a) From the upper edge of the band gap, $\mathcal{PT}$-soliton solutions move into the gap as the total energy E increases. (b) Width w of nonconservative solitons. (c) Total energy threshold and (d) maximum lifetime (in time step m) as a function of gain potential.

[see Fig. 4(d)]. For those $\mathcal{PT}$-symmetric low energy stationary soliton solutions that are relatively broad ($w \approx 5$ unit cells), their dimensions are noticeably larger than the step size of the lattice or its internal structure (under $\mathcal{PT}$-symmetric gain and phase modulation). As a result, discretization effects become negligible in this quasicontinuous limit, thus allowing these otherwise unstable solitons to live for very long propagation times given that the gain contrast factor is small [see Fig. 4(d)]. In all cases, as in 1D systems [25,26], we found that a 2D soliton exhibits a small energy growth that is proportional to the gain factor (G), despite the fact that $\mathcal{PT}$ symmetry of the lattice was restored in the linear limit—a clear indication that $\mathcal{PT}$ symmetry is locally broken by nonlinearity (see the Supplemental Material [31], Note 11). Furthermore, as non-Hermitian 2D solitons propagate in this quasiconservative system, they do not immediately disintegrate, but instead, their energy exponentially grows until they collapse. Unlike a 1D system, the rate of growth of this instability is further enhanced in a 2D environment—especially close to the collapse point where the $\mathcal{PT}$ symmetry is now violated.

By further increasing the input power, for instance 4.15 mW in this experiment, the region of instability is reached faster and nonlinear self-focusing leads to an immediate collapse of the field distribution, in a way analogous to what happens in a conservative 2D discrete Schröedinger system [27] [see Fig. 3(i)]. Unlike what happens in its conservative counterpart ($G = 1.0$) [28], the non-Hermitian collapse event is followed by a fast growth of the total energy [see red curve in Fig. 3(b)], which leads to an even stronger local break in the $\mathcal{PT}$ symmetry. This extremely localized field is concentrated around a single lattice site and a small amount of excess radiation is released in the form of outward propagating waves [see Figs. 3(i) and 3(j)]. During collapse, this highly localized wave nonlinearly self-accelerates and as a result moves on the lattice [see Fig. 3(k)]. Numerical simulations suggest that in most cases the directionality of this movement tends to be perpendicular to the zigzag-shaped $\mathcal{PT}$-phase potentials (PN barrier), meaning that the energy of the highly localized state is large enough to overcome this potential barrier. Nevertheless, due to its very small width ($w \approx 1$), this moving localized solution experiences discretization effects from the lattice as well as the previously mentioned zigzag-shaped $\mathcal{PT}$-phase potentials (see the Supplemental Material [31], Note 11). Consequently, by overcoming the phase barrier, this moving, highly localized, collapsed soliton gradually loses its energy and finally dissolves.

In conclusion, we successfully realized a novel $\mathcal{PT}$-symmetric system in a 2D synthetic lattice. By appropriately modulating the gain contrast as well as the pertinent phase, we experimentally investigate the non-Hermitian nonlinear localization of a broad Gaussian-like field distribution. In contrast to what one could expect from a Hermitian system, nonconservative $\mathcal{PT}$ solitons display an effective energy growth—a process that makes them more unstable and rapidly induces a collapse event. For higher input power levels, a family of non-Hermitian solitons is observed for the first time that tends to self-accelerate and move during collapse. Of further interest will be to study how correlated disorder influences these processes in 2D lattices—a regime where $\mathcal{PT}$ symmetry is linearly preserved.

This project was supported by the German Research Foundation (DFG) (GRK 2101) as well as an NSERC CREATE grant. This work was supported by the Office of Naval Research (N00014-18-1-2347), Army Research Office (W911NF-17-1-0481), Texas AM (NPRP9-020-1-006), Penn State MRSEC—Center for Nanoscale Science (1420620), Air Force Office of Scientific Research (FA9550-14-1-0037), Defense Advanced Research Projects Agency (HR00111820042, HR00111820038). P. S. J is grateful the Polish Ministry of Science and Higher Education for Mobility Plus scholarship. R. M. also acknowledges additional support by the Government of the Russian Federation through the ITMO Fellowship and Professorship Program (Grant No. 074-U 01) and by the 1000 Talents Sichuan Program in China.

*Corresponding author.
ulf.peschel@uni-jena.de
†Also at ITMO University, Kronverkskiy Prospekt 49, St. Petersburg 197101, Russia; Also at Institute of Fundamental and Frontier Science, University of Electronic Science and Technology of China, North Jianshe Road 4, Chengdu 610054, China.
‡Also at Faculty of Physics, Warsaw University of Technology, Koszykowa 75, 00-662 Warsaw, Poland.

[1] G. Agrawal, *Nonlinear Fiber Optics* (Academic Press, 2006), p. 87–128.
[2] G. Björk, A. Karlsson, and Y. Yamamoto, Definition of a laser threshold, Phys. Rev. A **50**, 1675 (1994).
[3] N. Moiseyev, *Non-Hermitian Quantum Mechanics* (Cambridge University Press, 2011), p. 211–247.
[4] R. El-Ganainy, K. G. Makris, M. Khajavikhan, Z. H. Musslimani, S. Rotter, and D. N. Christodoulides, Non-Hermitian physics and PT symmetry, Nat. Phys. **14**, 11 (2018).
[5] H. Ramezani, T. Kottos, R. El-Ganainy, and D. N. Christodoulides, Unidirectional nonlinear $\mathcal{PT}$-symmetric optical structures, Phys. Rev. A **82**, 043803 (2010).
[6] A. Regensburger, C. Bersch, M.-A. Miri, G. Onishchukov, D. N. Christodoulides, and U. Peschel, Parity-time synthetic photonic lattices, Nature (London) **488**, 167 (2012).
[7] H. Schomerus, Quantum Noise and Self-Sustained Radiation of $\mathcal{PT}$-Symmetric Systems, Phys. Rev. Lett. **104**, 233601 (2010).
[8] S. Longhi, $\mathcal{PT}$-symmetric laser absorber, Phys. Rev. A **82**, 031801(R) (2010).

[9] Z. Lin, H. Ramezani, T. Eichelkraut, T. Kottos, H. Cao, and D. N. Christodoulides, Unidirectional Invisibility Induced by $\mathcal{PT}$-Symmetric Periodic Structures, Phys. Rev. Lett. **106**, 213901 (2011).

[10] M. Kulishov, J. M. Laniel, N. Bélanger, J. Azaña, and D. V. Plant, Nonreciprocal waveguide Bragg gratings, Opt. Express **13**, 3068 (2005).

[11] L. Feng, Y.-L. Xu, W. S. Fegadolli, M.-H. Lu, J. E. B. Oliveira, V. R. Almeida, Y.-F. Chen, and A. Scherer, Experimental demonstration of a unidirectional reflectionless parity-time metamaterial at optical frequencies, Nat. Mater. **12**, 108 (2013).

[12] A. E. Miroshnichenko, B. A. Malomed, and Y. S. Kivshar, Nonlinearly $\mathcal{PT}$-symmetric systems: Spontaneous symmetry breaking and transmission resonances, Phys. Rev. A **84**, 012123 (2011).

[13] K. G. Makris, R. El-Ganainy, D. N. Christodoulides, and Z. H. Musslimani, Beam Dynamics in $\mathcal{PT}$ Symmetric Optical Lattices, Phys. Rev. Lett. **100**, 103904 (2008).

[14] M. Kremer, T. Biesenthal, L. J. Maczewsky, M. Heinrich, R. Thomale, and A. Szameit, Demonstration of a two-dimensional pt-symmetric crystal, Nat. Commun. **10**, 435 (2019).

[15] A. Szameit, M. C. Rechtsman, O. Bahat-Treidel, and M. Segev, $\mathcal{PT}$-symmetry in honeycomb photonic lattices, Phys. Rev. A **84**, 021806(R) (2011).

[16] M.-A. Miri, A. Regensburger, U. Peschel, and D. N. Christodoulides, Optical mesh lattices with $\mathcal{PT}$ symmetry, Phys. Rev. A **86**, 023807 (2012).

[17] M. Parto, S. Wittek, H. Hodaei, G. Harari, M. A. Bandres, J. Ren, M. C. Rechtsman, M. Segev, D. N. Christodoulides, and M. Khajavikhan, Edge-Mode Lasing in 1d Topological Active Arrays, Phys. Rev. Lett. **120**, 113901 (2018).

[18] Y. N. Joglekar, D. Scott, M. Babbey, and A. Saxena, Robust and fragile $\mathcal{PT}$-symmetric phases in a tight-binding chain, Phys. Rev. A **82**, 030103(R) (2010).

[19] E.-M. Graefe and H. F. Jones, $\mathcal{PT}$-symmetric sinusoidal optical lattices at the symmetry-breaking threshold, Phys. Rev. A **84**, 013818 (2011).

[20] C. E. Rüter, K. G. Makris, R. El-Ganainy, D. N. Christodoulides, M. Segev, and D. Kip, Observation of parity-time symmetry in optics, Nat. Phys. **6**, 192 (2010).

[21] A. Guo, G. J. Salamo, D. Duchesne, R. Morandotti, M. Volatier-Ravat, V. Aimez, G. A. Siviloglou, and D. N. Christodoulides, Observation of $\mathcal{PT}$-Symmetry Breaking in Complex Optical Potentials, Phys. Rev. Lett. **103**, 093902 (2009).

[22] S. Klaiman, U. Günther, and N. Moiseyev, Visualization of Branch Points in $\mathcal{PT}$-Symmetric Waveguides, Phys. Rev. Lett. **101**, 080402 (2008).

[23] Y. D. Chong, L. Ge, and A. D. Stone, $\mathcal{PT}$-Symmetry Breaking and Laser-Absorber Modes in Optical Scattering Systems, Phys. Rev. Lett. **106**, 093902 (2011).

[24] B. Midya, B. Roy, and R. Roychoudhury, A note on the pt invariant periodic potential $\mathrm{v}(\mathrm{x}) = 4\cos 2\mathrm{x} + 4\mathrm{iv}0\sin 2\mathrm{x}$, Phys. Lett. A **374**, 2605 (2010).

[25] M. Wimmer, A. Regensburger, M.-A. Miri, C. Bersch, D. N. Christodoulides, and U. Peschel, Observation of optical solitons in pt-symmetric lattices, Nat. Commun. **6**, 7782 (2015).

[26] S. V. Suchkov, A. A. Sukhorukov, J. Huang, S. V. Dmitriev, C. Lee, and Y. S. Kivshar, Nonlinear switching and solitons in pt-symmetric photonic systems, Laser Photonics Rev. **10**, 177 (2016).

[27] C. Sulem and P. L. Sulem, The nonlinear Schrodinger equation: self-focusing and wave collapse, Appl. Math. Sci. **139**, 141 (1999).

[28] A. L. M. Muniz, M. Wimmer, A. Bisianov, R. Morandotti, and U. Peschel, Collapse on the line how synthetic dimensions influence nonlinear effects, Sci. Rep. **9**, 9518 (2019).

[29] L. Yuan, Q. Lin, M. Xiao, and S. Fan, Synthetic dimension in photonics, Optica **5**, 1396 (2018).

[30] A. Schreiber, A. Gábris, P. P. Rohde, K. Laiho, M. Štefaňák, V. Potoček, C. Hamilton, I. Jex, and C. Silberhorn, A 2d quantum walk simulation of two-particle dynamics, Science **336**, 55 (2012).

[31] See the Supplemental Material at http://link.aps.org/supplemental/10.1103/PhysRevLett.123.253903 for the experimental setup, synthetic dimension technique, PT symmetry operators, amplitude and phase modulation, and numerical analysis.

[32] A. Schreiber, K. N. Cassemiro, V. Potoček, A. Gábris, P. J. Mosley, E. Andersson, I. Jex, and C. Silberhorn, Photons Walking the Line: A Quantum Walk with Adjustable Coin Operations, Phys. Rev. Lett. **104**, 050502 (2010).

[33] K. Mochizuki, D. Kim, and H. Obuse, Explicit definition of $\mathcal{PT}$ symmetry for non-unitary quantum walks with gain and loss, Phys. Rev. A **93**, 062116 (2016).

[34] M. Wimmer, A. Regensburger, C. Bersch, M.-A. Miri, S. Batz, G. Onishchukov, D. N. Christodoulides, and U. Peschel, Optical diametric drive acceleration through actionreaction symmetry breaking, Nat. Phys. **9**, 780 (2013).

[35] A. Regensburger, C. Bersch, B. Hinrichs, G. Onishchukov, A. Schreiber, C. Silberhorn, and U. Peschel, Photon Propagation in a Discrete Fiber Network: An Interplay of Coherence and Losses, Phys. Rev. Lett. **107**, 233902 (2011).

[36] L. Grüner-Nielsen, M. Wandel, P. Kristensen, C. Jorgensen, L. V. Jorgensen, B. Edvold, B. Pálsdóttir, and D. Jakobsen, Dispersion-compensating fibers, J. Lightwave Technol. **23**, 3566 (2005).

[37] D. F. V. James, P. G. Kwiat, W. J. Munro, and A. G. White, Measurement of qubits, Phys. Rev. A **64**, 052312 (2001).

[38] Y. S. Kivshar and D. K. Campbell, Peierls-nabarro potential barrier for highly localized nonlinear modes, Phys. Rev. E **48**, 3077 (1993).

[39] A. Gómez-León and G. Platero, Floquet-Bloch Theory and Topology in Periodically Driven Lattices, Phys. Rev. Lett. **110**, 200403 (2013).

[40] K. D. Moll, A. L. Gaeta, and G. Fibich, Self-Similar Optical Wave Collapse: Observation of the Townes Profile, Phys. Rev. Lett. **90**, 203902 (2003).

[41] M. Johansson, J. E. Prilepsky, and S. A. Derevyanko, Strongly localized moving discrete dissipative breather-solitons in kerr nonlinear media supported by intrinsic gain, Phys. Rev. E **89**, 042912 (2014).